Short Article

Cell Metabolism

Regulation of Mother-to-Offspring Transmission of mtDNA Heteroplasmy

Graphical Abstract

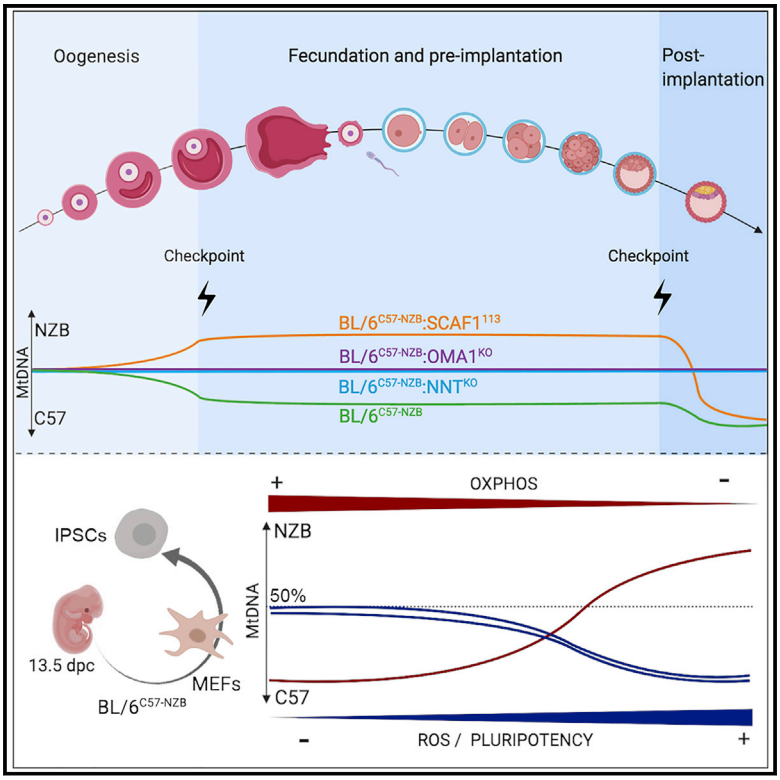

Highlights

- Wild-type mtDNA heteroplasmy is sensed in oocyte maturation and embryo development
- Random versus selective mtDNA segregation is driven by the nuclear genetic context
- Haplotype-derived OXPHOS differences and ROS signaling define the preferred mtDNA
- Efficiency of iPSC generation strongly depends on the mtDNA haplotype

Authors

Ana Latorre-Pellicer,
Ana Victoria Lechuga-Vieco,
Iain G. Johnston, ..., Nick S. Jones,
Jesús Ruíz-Cabello,
José Antonio Enríquez

Correspondence

jaenriquez@cnic.es

In Brief

The dynamics of heteroplasmic mtDNA populations and the factors that promote mtDNA homogeneity remain poorly understood. Latorre-Pellicer et al. have discovered that heteroplasmy is checked at oocyte maturation and in the early embryo. mtDNA segregation can occur on a spectrum from random drift to strong selection of one of the haplotypes, through mechanisms dependent upon mito-nuclear interactions affecting embryo metabolism and cell fitness.

Latorre-Pellicer et al., 2019, Cell Metabolism *30*, 1120–1130
December 3, 2019 Crown Copyright © 2019 Published by Elsevier Inc.
https://doi.org/10.1016/j.cmet.2019.09.007

CellPress

Cell Metabolism
Short Article

Regulation of Mother-to-Offspring Transmission of mtDNA Heteroplasmy

Ana Latorre-Pellicer,[1,2,12] Ana Victoria Lechuga-Vieco,[1,3,12] Iain G. Johnston,[4] Riikka H. Hämäläinen,[5,6] Juan Pellico,[1,3] Raquel Justo-Méndez,[1] Jose María Fernández-Toro,[1] Cristina Clavería,[1] Adela Guaras,[1] Rocío Sierra,[1] Jordi Llop,[7,8] Miguel Torres,[1] Luis Miguel Criado,[1] Anu Suomalainen,[6] Nick S. Jones,[9] Jesús Ruíz-Cabello,[3,7,8,10] and José Antonio Enríquez[1,11,13,*]

[1]Centro Nacional de Investigaciones Cardiovasculares Carlos III, Madrid, Spain
[2]Unit of Clinical Genetics and Functional Genomics, Department of Pharmacology-Physiology, School of Medicine, University of Zaragoza, ISS-Aragon, 50009 Zaragoza, Spain
[3]CIBERES: C/ Melchor Fernández-Almagro 3, 28029 Madrid, Spain
[4]School of Biosciences, University of Birmingham, Birmingham, UK
[5]Department of Neurobiology, A.I. Virtanen Institute for Molecular Sciences, University of Eastern Finland, Kuopio, Finland
[6]Research Program of Molecular Neurology, Biomedicum, University of Helsinki, Helsinki, Finland
[7]CIC biomaGUNE, Paseo Miramón No 182, San Sebastián, 20014 Guipúzcoa, Spain
[8]IKERBASQUE, Basque Foundation for Science, Bilbao, Spain
[9]Department of Mathematics, Imperial College London, London SW7 2BB, UK
[10]Universidad Complutense de Madrid, Madrid 28606, Spain
[11]CIBERFES: C/ Melchor Fernández-Almagro 3, 28029 Madrid, Spain
[12]These authors contributed equally
[13]Lead Contact
*Correspondence: jaenriquez@cnic.es
https://doi.org/10.1016/j.cmet.2019.09.007

SUMMARY

mtDNA is present in multiple copies in each cell derived from the expansions of those in the oocyte. Heteroplasmy, more than one mtDNA variant, may be generated by mutagenesis, paternal mtDNA leakage, and novel medical technologies aiming to prevent inheritance of mtDNA-linked diseases. Heteroplasmy phenotypic impact remains poorly understood. Mouse studies led to contradictory models of random drift or haplotype selection for mother-to-offspring transmission of mtDNA heteroplasmy. Here, we show that mtDNA heteroplasmy affects embryo metabolism, cell fitness, and induced pluripotent stem cell (iPSC) generation. Thus, genetic and pharmacological interventions affecting oxidative phosphorylation (OXPHOS) modify competition among mtDNA haplotypes during oocyte development and/or at early embryonic stages. We show that heteroplasmy behavior can fall on a spectrum from random drift to strong selection, depending on mito-nuclear interactions and metabolic factors. Understanding heteroplasmy dynamics and its mechanisms provide novel knowledge of a fundamental biological process and enhance our ability to mitigate risks in clinical applications affecting mtDNA transmission.

INTRODUCTION

Mitochondrial DNA (mtDNA) exists in populations within eukaryotic cells and encodes genes that are vital for cellular energetics and metabolism. Cellular populations of mtDNA may be genetically identical (homoplasmy) or consist of a genetic admixture (heteroplasmy) arising from mutation, inheritance, or gene therapies. The interaction between different variants of mtDNA within the same cytoplasm is a fascinating biological problem with evolutionary, physiological, pathological, and ethical implications. It has

Context and Significance

Normally, one single version of mtDNA is present in a cell. Recent observations indicate that more than one mtDNA variant would be present in the same cell (heteroplasmy). Latorre-Pellicer et al. have investigated this phenomenon across generations in mice harboring two versions of mtDNA. During early embryo development and oogenesis, the cell can detect the mtDNA variants and selectively expand one of them until it becomes predominant. The selection process is dependent upon specific nuclear-encoded genes and their interaction with mitochondrial genes. This information on the regulation of heteroplasmy may be used to prevent the transmission of mtDNA-linked diseases and to better design medical technologies that involve mitochondrial transfer from a donor.

come to the forefront of public awareness due to debate concerning the use of mitochondrial replacement therapy in human oocytes to prevent transmission of mtDNA-linked diseases (Tachibana et al., 2009; Craven et al., 2010), and the proposal to improve fertility by injecting young donor oocyte cytoplasm and mtDNA to oocytes of sub-fertile women (Woods and Tilly, 2015). However, the dynamics of heteroplasmic mtDNA populations and the factors that affect these dynamics remain poorly understood.

In mammals, mtDNA encodes a reduced number of genes: 13 mRNAs, 22 tRNAs, and 2 rRNAs. All proteins encoded in the mtDNA are structural components of the multiprotein mitochondrial respiratory complexes. It is critical that these mtDNA-encoded proteins match physically and functionally with up to 70 nDNA-encoded structural proteins of the same complexes to build a functional oxidative phosphorylation (OXPHOS) system. Animal models with identical nuclear genomes but with different mtDNA haplotypes (conplastic mice) generate functionally different OXPHOS systems that shape organismal metabolism (Latorre-Pellicer et al., 2016), supporting the conclusion that different wild-type mtDNA variants have phenotypically important consequences.

Selection between non-pathological mtDNA haplotypes in the female germline of heteroplasmic engineered mice was first thought not to exist (Jenuth et al., 1996), but this conclusion has been recently questioned (Burgstaller et al., 2014; Sharpley et al., 2012). Solving this dispute is of major interest in addressing the potential medical implications of mixed mtDNA populations. The analysis of mtDNA heteroplasmy progression in genetically manipulated monkey heteroplasmic oocytes revealed that, during embryo development, one of the mtDNA variants may become predominant (Lee et al., 2012). In human embryonic stem cells (ESCs) derived from embryos cultured *in vivo* after nuclear transfer to exchange mtDNA complements, similar expansion of the residual mtDNA haplotype has been observed (Kang et al., 2016; Yamada et al., 2016). Very recently, expansion of the minority copies of paternal mtDNA (70 versus 200,000) was documented in human families where the active elimination of the sperm mitochondria failed (Luo et al., 2018). The driving forces responsible for the selective advantage of mtDNA during embryo development is still unknown.

Here, we address these questions by elucidating mtDNA behavior between non-pathological mtDNA variants in unprecedented detail in a set of novel model organisms. We identify stages at which mtDNA haplotype selection occurs during early embryo development and a set of metabolic and nuclear genetic factors that drive this selection.

RESULTS

mtDNA Competition at Early Embryonic Stages

We generated heteroplasmic mice by electro-fusion of an embryo and an enucleated embryo. The nuclear genome from C57BL/6JOlaHsd strain was combined with mtDNA either of NZB/OlaHsd (BL/6^{NZB}) or of C57BL/6JOlaHsd (BL/6^{C57}). The heteroplasmic offspring (named BL/6$^{C57\text{-}NZB}$) were mated with C57BL/6JOlaHsd males to prevent nuclear genetic drift in our particular mice strains. We did not observe any adverse effect of the heteroplasmy in ovary, embryo development, or fertility (Figures S1A and S1B). Only the offsprings of the established heteroplasmic mice were used.

During female germline maturation, mtDNA undergoes a genetic bottleneck where random drift and positive selection may both act to strongly reduce heteroplasmy in cells (Johnston et al., 2015). A parallel assessment of heteroplasmy in gonads (ovary and testis) and in germline cells revealed that both oocytes and spermatozoa progressively select for C57 mtDNA with age despite their rather dissimilar differentiation process (Figures 1A and 1B). Oocytes are the cells with the highest mtDNA content, up to 200,000 copies per cell (Pikó and Taylor, 1987), while sperm mtDNA content is among the lowest (70 copies per cell) (Díez-Sánchez et al., 2003). Whole-ovary analysis also showed a significant tendency to accumulate C57 mtDNA while testes accumulated NZB mtDNA (Figures 1A and 1B). Therefore, the mtDNA extracted from ovaries is a good proxy of the behavior of the oocyte mtDNA heteroplasmy, whereas the analysis of testis cannot inform us about the sperm mtDNA heteroplasmy.

How does this selection of C57 mtDNA in ovaries occur? In fetal stage, during early oogenesis, there is a substantial increase in mtDNA copy number (10 to 20 times [Wai et al., 2008]). Post-natal maturation of the oocytes for ovulation requires a further mtDNA replication activity with a burst in mtDNA copy number (Johnston et al., 2015; Wai et al., 2008). Analysis of the ovary at different ages of the mother showed that the mtDNA haplotype (C57 or NZB) modifies the proportion of follicles at different stages of maturation, with a better maintenance of the ovary function with NZB mtDNA. In particular, the proportion of primordial follicles at early age is increased in the presence of NZB mtDNA with respect to that shown in homoplasmic C57 mtDNA (Figure S1C). Heteroplasmy induces an accelerated loss of primary oocytes (Figure S1C). This loss may suggest either a selection against subpopulations of follicles with higher proportion of NZB mtDNA or, alternatively, an earlier maturation of oocytes with higher content of NZB mtDNA. However, additional mtDNA intracellular selection within oocytes with age can also occur. Either scenario could explain the shift in heteroplasmy toward more C57 mtDNA with the age of the mother. Wai and Shoubridge (Wai et al., 2008) reported a significant increase in NZB mtDNA in more mature oocytes when studying heteroplasmy dynamics (Balb/c versus NZB mtDNA haplotypes) between primary follicles and secondary follicles (between post-natal day 1 and post-natal day 29), but this observation cannot rule out the alternative explanations. Moreover, the analysis of over 900 pups reveal that the C57 mtDNA is significantly favored, with a 45:1 proportion of homoplasmic C57 versus NZB (Figure 1C).

Based on these heteroplasmy changes observed in ovaries, the intergenerational heteroplasmy shift between mother and offspring (measured by comparing tail measurements at day 21) was predicted to increase with the mother's age at pup birth. Our observations indeed indicate a selective segregation in favor of C57 mtDNA haplotype from heteroplasmic mothers to pups (Figure 1C). However, the female germline segregation inferred through ovary mtDNA dynamics cannot account in full for the observed mother-to-pup shift in mtDNA heteroplasmy (Figure 1C), suggesting that additional selection in favor of C57 mtDNA haplotype takes place during gestation.

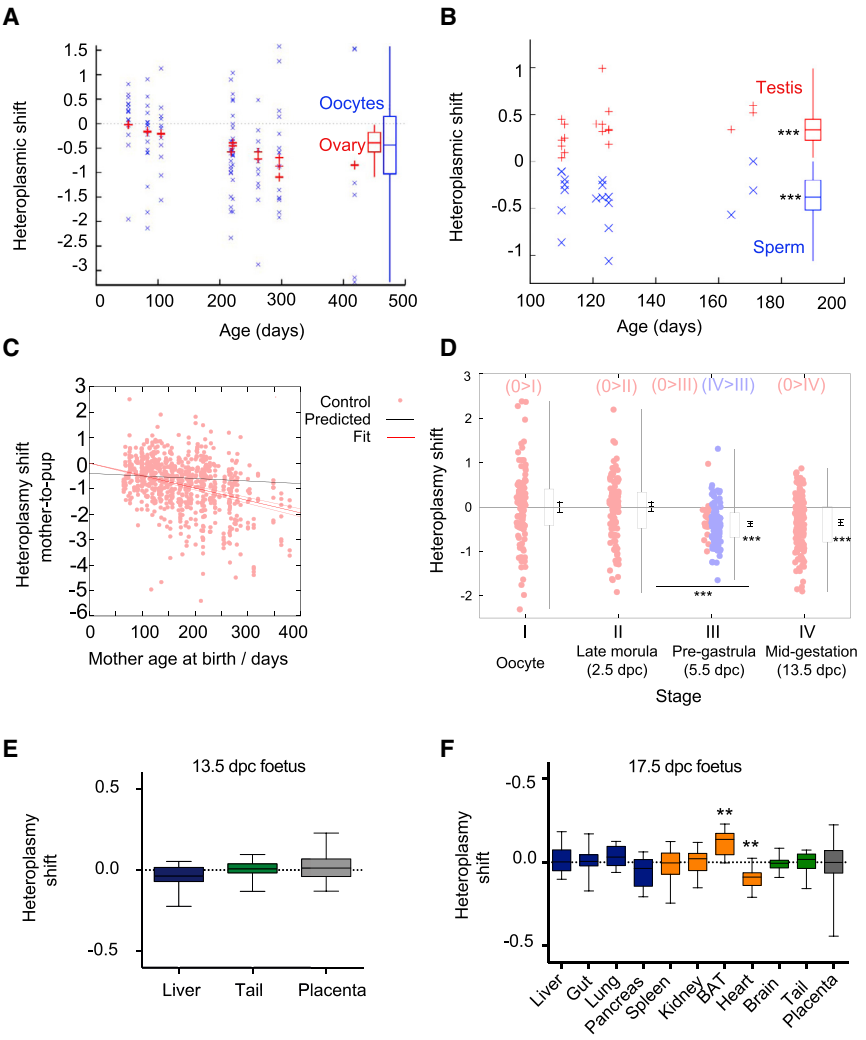

Figure 1. Heteroplasmy Is Sensed and mtDNA Segregated Prenatally

(A) Convergence in heteroplasmic proportions between ovary (red, $p = 1.2 \times 10^{-4}$ against zero segregation) and oocytes (blue, $p = 3.7 \times 10^{-4}$ against zero segregation) (n = 110 oocytes and n = 13 ovaries from 13 BL/6$^{C57\text{-}NZB}$ females).

(B) Divergence in the heteroplasmic proportion between testis (red, $p = 7.6 \times 10^{-6}$ against zero segregation) and spermatozoa (blue, $p = 1.5 \times 10^{-4}$ against zero segregation) (n = 18).

In (A) and (B), the candlesticks show heteroplasmy statistics amalgamated over time, compared to a zero-change null hypothesis.

(C) Heteroplasmy shift between mother's tail sampled at 21 days old and pup's tail sampled at 21 days old (vertical axis), as a function of the mother's age when the pup was born (horizontal axis). Red lines show a fit, with 95% CI, to a linear decrease in transformed heteroplasmy (STAR Methods) with mother's age. Black line shows the predicted trend from the inferred developmental shift and ovarian segregation; alone, it cannot explain the observed shift in heteroplasmy between mothers and their offspring (pups = 819 from 43 BL/6$^{C57\text{-}NZB}$ females, ovary = 73 from BL/6$^{C57\text{-}NZB}$ females).

(D) Shifts in heteroplasmy, relative to ovary heteroplasmy, observed upon a change into each pluripotency class. The classes are 0 (ovary, n = 73), I (oocyte, n = 110), II (2.5 dpc embryos, n = 101), III (5.5 dpc embryos, n = 21, $p = 1.0 \times 10^{-13}$ against zero segregation, $p = 4.7 \times 10^{-6}$ against identity to II), and IV (13.5 dpc embryos, n = 161, $p = 3.0 \times 10^{-9}$ against zero segregation). Pink dots represent heteroplasmy level in the indicated embryo class samples, and blue dots represent heteroplasmy in iPSCs derived from MEF lines stablished from class IV embryos. Heteroplasmy changes are tested against a zero-change null hypothesis, and between classes.

(E and F) Variability in heteroplasmy between embryos of the same litter at 13.5 (n = 9) (E) or 17.5 dpc (n = 10) (F) and between the indicated tissues.

In (A)–(C), (E), and (F), transformed heteroplasmy shift using tail as the reference tissue. In (E) and (F), comparisons assessed by Mann-Whitney test and one-way ANOVA; Tukey's range test correction for multiple comparison (*$p < 0.05$; **$p < 0.01$; ***$p < 0.001$).

Pursuing this observation, we found that a very fast shift in heteroplasmy happened during early development between 2.5 and 5.5 days post-coitum (dpc), which includes the implantation and pre-gastrula post-implantation stages (Figure 1D). No evidence of selection could be observed between 5.5 and 13.5 dpc embryos (Figures 1D, 1E, and S1D). At 17.5 dpc, heart and brown adipose tissue (BAT) revealed selection in favor of C57 and NZB mtDNAs respectively (Figures 1F and S1D). Interestingly, placenta did not show any mtDNA haplotype preference at any stage.

In summary, mother-to-pup development of heteroplasmy has dual contributions, both from positive selection for C57 in developing oocytes and additional positive selection in early embryogenesis. This dual selection mirrors the dynamics observed in another heteroplasmic mouse model (Burgstaller et al., 2018).

Heteroplasmy Alters Metabolism of Mouse Embryonic Fibroblast and of the Embryo

We next asked whether metabolic factors may be responsible for these mtDNA selection patterns. Recently, we demonstrated that the two mtDNA variants (NZB or C57) determine qualitatively different OXPHOS performance in mice (Latorre-Pellicer et al., 2016), confirming our previous observations in cybrid cell lines (Moreno-Loshuertos et al., 2006). To investigate whether such variations in OXPHOS function influence mtDNA haplotype segregation, we isolated mouse embryonic fibroblasts (MEFs) from post-implantation embryos of the homoplasmic strains, BL/6^{C57} and BL/6^{NZB}, and from heteroplasmic mice, BL/6$^{C57\text{-}NZB}$, with three different proportions of heteroplasmy (Figure 2). To guarantee that they were true heteroplasmic cells and not a mix of cells with different mtDNAs, heteroplasmy was assessed using padlock probes to detect *in situ* each mitochondrial DNA haplotype by confocal fluorescence microscopy. In this way, we could conclude that heteroplasmy is intracellular and not intercellular (Figure 2A), as both mtDNA variants co-exist in the same cytoplasm.

Interestingly, heteroplasmic MEFs showed a consistent reduction in basal and maximum respiration capacity, regardless of the proportion of heteroplasmy and the carbon source (Figures 2B and 2C). The presence of any level of heteroplasmy

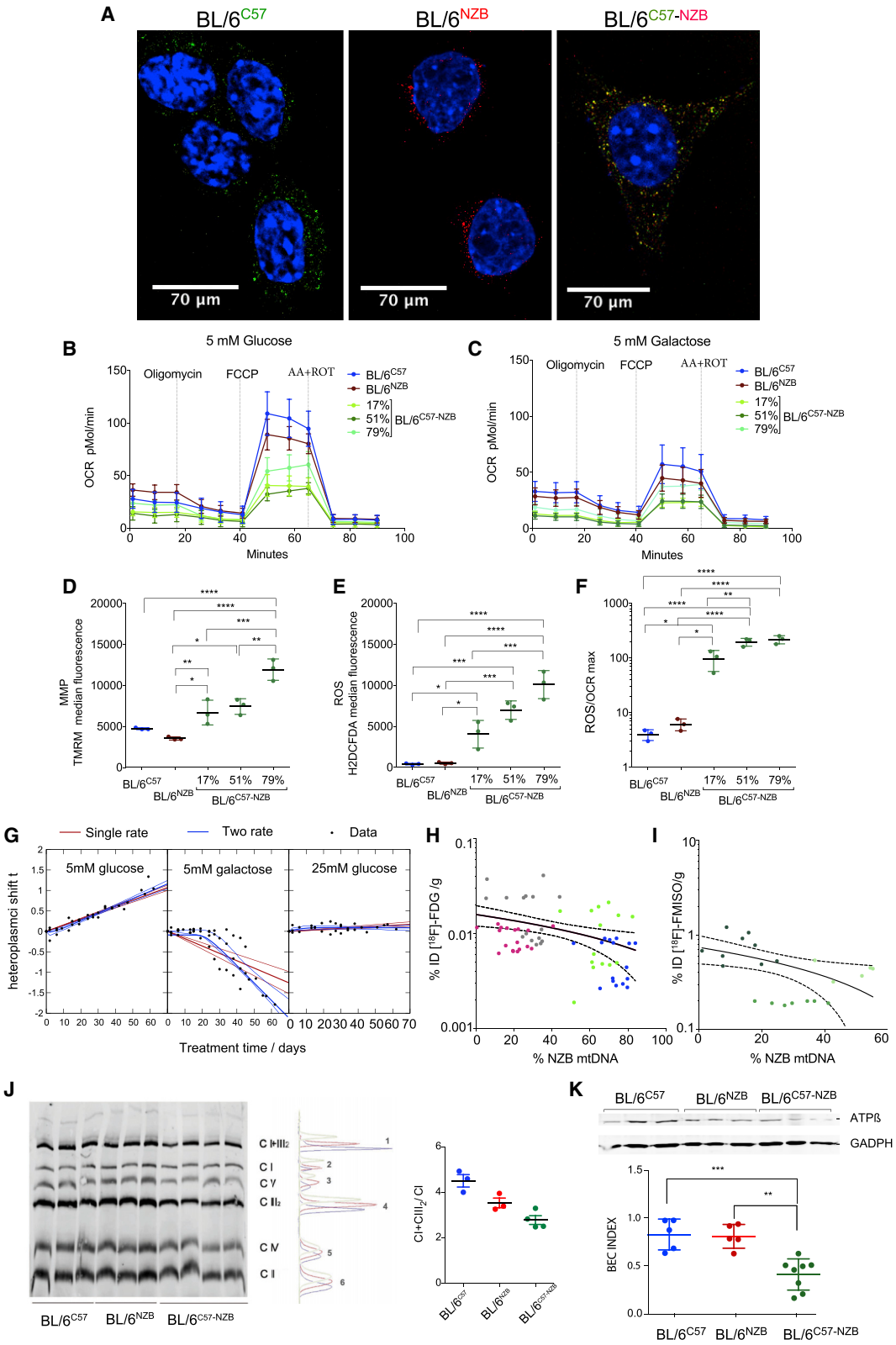

(legend on next page)

induced elevated mitochondrial membrane potential (MMP) (Figure 2D) and higher reactive oxygen species (ROS) production (Figure 2E), one order of magnitude higher than the homoplasmic MEFs when normalized by the maximum respiration rate (MRR) (Figure 2F). We further observed that these functional consequences feed back onto the dynamics of mtDNA populations. MEFs maintained heteroplasmy levels when grown in glucose over-rich medium, whereas they favored NZB mtDNA at physiological concentrations of glucose and shifted toward C57 mtDNA in a medium promoting OXPHOS, when glucose was substituted by galactose (Figures 2G and S1E).

Following these observations, we asked whether these metabolic impacts of heteroplasmy in cultured MEFs reflected similar impacts *in vivo*. We investigated the metabolic poise of 12.5 dpc embryos by determining their ability to uptake ^{18}F-Fluorodeoxyglucose ([^{18}F]-FDG) or ^{18}F-Fluoromisonidazole ([^{18}F]-FMISO) using positron emission tomography and computed tomography (PET-CT). In addition, we quantified the uptake of the probes by gamma counter in isolated embryos. In this way, we could estimate the embryo glucose demands ([^{18}F]-FDG) and oxygen utilization in correlation with their heteroplasmy proportion. Notice that the ([^{18}F]-FMISO) is an inverse indicator of oxygen consumption since the signal increase in hypoxic status (Grimes et al., 2017; Corroyer-Dulmont et al., 2015; Warren and Partridge, 2016). We found that glucose uptake is decreased (Figures 2H and S1F) and oxygen level higher (Figures 2I, S1G, and S1H) when NZB mtDNA predominates (Figure S1H; 100% NZB mtDNA). This observation in the embryo is reminiscent of our previous results showing that NZB and C57 mtDNAs promote differential organismal metabolism (Latorre-Pellicer et al., 2016). The PET-CT analysis indicates that the energetic metabolism of the embryos, with high glycolytic predominance, can be modulated between more oxidative versus more glycolytic metabolism (Figures 2H, 2I, and S1H).

We next sought to characterize the influence of mtDNA population structure on metabolic poise at a finer-grained, molecular scale. To this end, we isolated 12.5 dpc embryos from the homoplasmic and heteroplasmic strains and analyzed the organization of the mitochondrial electron transport chain by blue native electrophoresis (BNE). We found that the CI + $CIII_2$/CI ratio is decreased in homoplasmic NZB animals with respect to homoplasmic C57 (Figure 2J). We described elsewhere that in most C57BL/6 tissues, respiratory complex I is mainly distributed between the free monomer CI and the super-assembled CI + $CIII_2$ (Cogliati et al., 2016). We also showed that the relative ratio of CI + $CIII_2$/CI is adapted by the mitochondria according to available fuel, being higher when glutamate or pyruvate is the main source of electrons and reduced when fatty acids are the predominant source (Guarás et al., 2016). The substitution of C57 by NZB haplotype in homoplasmic animals induced a shift in the fuel use by mitochondria in adult liver and also reduces the CI + $CIII_2$/CI ratio (Latorre-Pellicer et al., 2016). In heteroplasmic embryos, we observed an exacerbated decrease in the CI + $CIII_2$/CI compared to homoplasmic NZB embryos (Figure 2J).

Looking at another molecular-scale readout of metabolic poise, we next assessed the relative contribution of glycolytic versus oxidative ATP production in the embryos by determining the bioenergetic cellular (BEC) index (Cuezva et al., 2004). The BEC index is calculated by the estimation of the ratio of expression between the beta subunit of the mitochondrial H^+-ATP synthase and a critical protein of the glycolysis (GAPDH) by western blot. This index was decreased in heteroplasmic versus homoplasmic embryos suggesting, as it was observed in MEFs, that heteroplasmy impacts on the mitochondrial OXPHOS efficiency (Figure 2K).

Thus, once more, we find that the presence of heteroplasmy has a qualitatively different effect on the metabolic poise of MEFs and embryos than would be expected as a simple combination of homoplasmic contributions.

Embryonic mtDNA Segregation Is Associated with Pluripotency

Despite the metabolic impact of mtDNA heteroplasmy on MEFs and embryos during gestation, dynamic changes in heteroplasmy seem largely restricted to a short period in early development. Since the observed stages of the segregation coincide with the appearance of pluripotency in the embryo epiblast, we decided to study the relationship between mtDNA heteroplasmy and pluripotency. We generated induced pluripotent stem cells (iPSCs) from BL/6^{C57}, BL/6^{NZB}, and heteroplasmic BL/6$^{C57\text{-}NZB}$ MEFs in order to reprogram their differentiation status toward pluripotency. Interestingly, cultured BL/6$^{C57\text{-}NZB}$ iPSCs strongly selected against NZB mtDNA (Figure 3A). Unexpectedly, we noticed a significant decrease in the reprogramming efficiency

Figure 2. Heteroplasmy Modulates MEF and Embryonic Metabolism

(A) Identification of C57 and NZB mtDNA haplotypes in MEFs by *in situ* fluorescence. In blue is labeled the nucleus; in green, mtDNA C57; in red, mtDNA NZB.

(B–F) Metabolic performance of MEFs derived from 12.5 dpc embryos of homoplasmic or heteroplasmic mice. Heteroplasmy indicates % of NZB mtDNA. Oxygen consumption rate (OCR) of intact cells estimated by SeaHorse at (B) 5 mM glucose and (C) 5 mM galactose. (D) Mitochondrial membrane potential and (E) H_2O_2 production per cell or (F) per maximum respiration (OCR) capacity.

(G) Dynamics of mtDNA segregation in MEFs under different nutritional conditions: 25 mM glucose displays no segregation (right); 5 mM glucose displays linear segregation (left); galactose shows significant support for a model where there is no heteroplasmy change in early treatment, followed by fast decrease after 21 days (center, likelihood ratio test, $p < 0.05$) (n = 3 BL/6$^{C57\text{-}NZB}$ immortalized MEF lines per treatment during 62 days of culture. Initial heteroplasmy levels: 43, 46, and 47% of NZB mtDNA respectively).

(H and I) Determination of [^{18}F]-FDG (H) or [^{18}F]-FMISO (I) uptake measured by gamma counter in 12.5 dpc embryos with different degrees of heteroplasmy. Each dot represents an individual embryo; colors indicate embryos from the same litter.

(J) BNE showing the assembly and superassembly status of respiratory complexes in the indicated 12.5 dpc embryos (left) and the proportion of the CI superassembly status (right) (n = 3 homoplasmic embryos and n = 4 heteroplasmic embryos).

(K) Western blot (top) and metabolic BEC index (ATPB/GADPH) quantification (bottom) of the relative proportion of glycolytic versus oxidative capacity in the indicated embryo strains (n = 5 homoplasmic embryos and n = 8 heteroplasmic embryos) (mean ± SD, one-way ANOVA test, *$p < 0.05$; **$p < 0.01$; ***$p < 0.001$; ****$p < 0.0001$).

See Tables S1 and S2 for antibodies utilized in western blot and padlock probes, respectively.

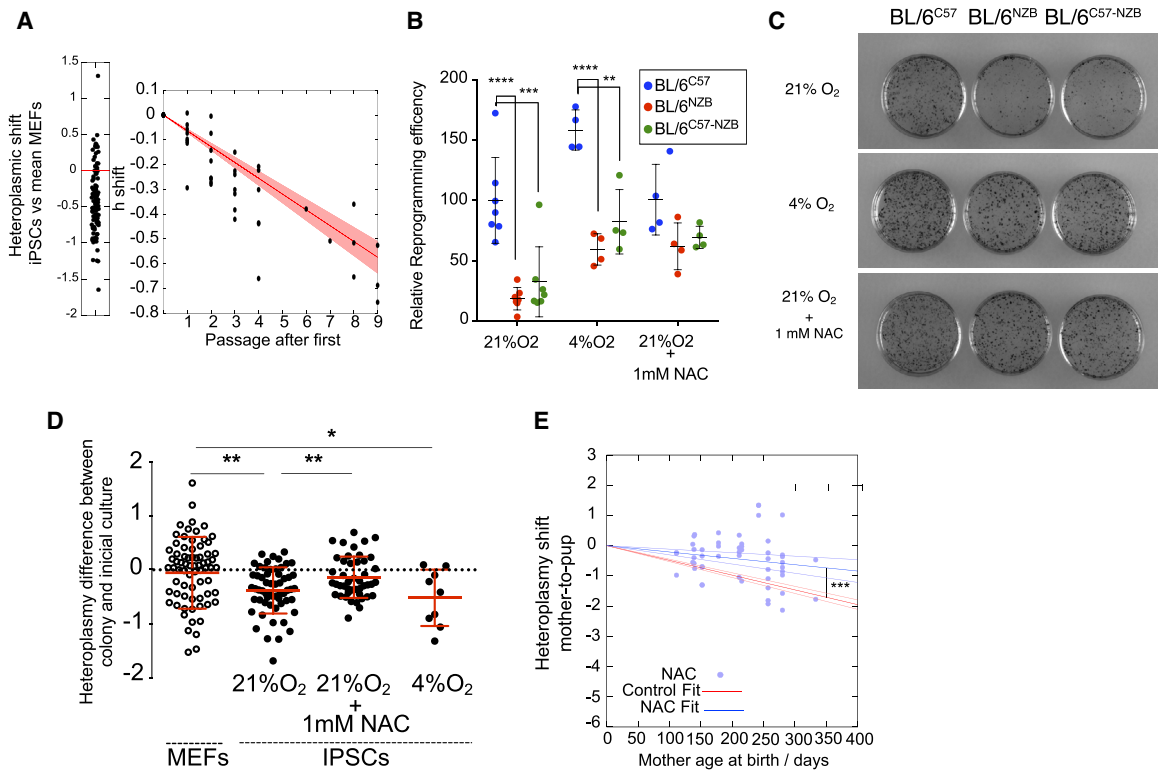

Figure 3. Heteroplasmy Modulates Pluripotency

(A) Left: heteroplasmy shift between the mean of the MEF set and individual derived iPSCs, showing a significant departure from zero (n = 80 iPSCs clones from 4 different MEFs BL/6$^{C57-NZB}$ lines, p = 1.4 × 10^{-11} against zero segregation). Heteroplasmy change with iPSC passage, with the heteroplasmy of the first passage as the reference value, and the x axis labeling subsequent passages (n = 8 iPSCs BL/6$^{C57-NZB}$ lines); lines show mean linear fit and 95% CI.

(B) iPSC reprogramming efficiency of BL/6^{C57}, BL/6^{NZB}, and BL/6$^{C57-NZB}$ MEFs under 21% O_2 (n = 7 per genotype), 21% O_2 (n = 4 per genotype) plus 1 mM NAC, and 4% O_2 (n = 4 per genotype) (mean ± SD, two-tailed t test, *p < 0.05; **p < 0.01; ***p < 0.001).

(C) Alkaline phosphatase (AP) staining of iPSC colonies 14 days after transposon-mediated gene transfer.

(D) Heteroplasmy shift between the mean of the MEFs set and individual MEFs, individual iPSCs reprogrammed under 21% O_2 (n = 50 iPSC clones), 21% O_2 plus 1 mM NAC (n = 45 iPSC clones), and 4% O_2 (n = 9 iPSC clones) (mean ± SD, ANOVA test, *p < 0.05; **p < 0.01).

(E) Heteroplasmy shift between mother and pups for mice treated with NAC. Red lines show the fit to a linear decrease in transformed heteroplasmy with mother's age from untreated animals (control mean and CI obtained from Figure 1C data points). Blue lines show a fit with 95% CI to the heteroplasmy shift between mother tail at 21 dpc and pups at 21 dpc with NAC administration in drinking water to mother during gestation (n = 52 pups from 9 BL/6$^{C57-NZB}$ females treated with NAC).

of MEFs obtained from conplastic BL/6^{NZB} and heteroplasmic BL/6$^{C57-NZB}$ animals when compared with MEFs from BL/6^{C57} mice (Figures 3B and 3C). These results are in agreement with a theoretical study elucidating the dependence of pluripotency on mitochondrial status (Johnston et al., 2012) and resemble what was reported for mutator mice that carry a load of mtDNA heteroplasmy (Hämäläinen et al., 2015). Moreover, we observed that NZB mtDNA was preferentially lost upon reprogramming of BL/6$^{C57-NZB}$ MEFs (Figure 3D). Using culture conditions with 4% oxygen, the reprogramming efficiency increased in MEFs regardless of their mtDNA content, but oxygen concentration did not prevent the heteroplasmic shift (Figures 3B and 3D).

We demonstrated elsewhere that the primary difference induced by the interchange of the mtDNA haplotypes NZB and C57 is the higher ROS signaling generated by NZB mtDNA (Latorre-Pellicer et al., 2016; Moreno-Loshuertos et al., 2006). Here, we found that heteroplasmic MEFs generate high levels of ROS (Figures 2E and 2F). To pursue the potential role of ROS in reprogramming, we generated iPSCs in the presence of 1 mM N-acetyl-L-cysteine (NAC), an antioxidant and reductant. We found that reprogramming efficiency increased significantly in MEFs derived from BL/6^{NZB} and BL/6$^{C57-NZB}$ embryos without affecting that of BL/6^{C57} MEFs (Figures 3B and 3C). Moreover, the presence of NAC eliminated the heteroplasmic shift during MEFs to iPSCs reprogramming (Figure 3D). Overall, this behavior is reminiscent of the observed reduction in iPSCs reprogramming efficiency associated with elevated mitochondrial ROS and the demonstration of negative selection against mutant mtDNA by pluripotent stem cells (Hämäläinen et al., 2015). Remarkably, per-oral NAC treatment provided to the BL/6$^{C57-NZB}$ pregnant females in their drinking water abolished the observed early embryonic shift in heteroplasmy (Figure 3E). In the presence of NAC, the mtDNA selection during oocyte maturation can account in full for the heteroplasmic shift between the mother and pups (Figure 3E).

These results suggest that mtDNA haplotype has a substantial effect on reprogramming efficiency and pluripotency of cells, which likely manifest at least in part by levels of ROS production, and reminiscent of the above feedback loops, the differentiation process places selective pressure on cellular mtDNA populations.

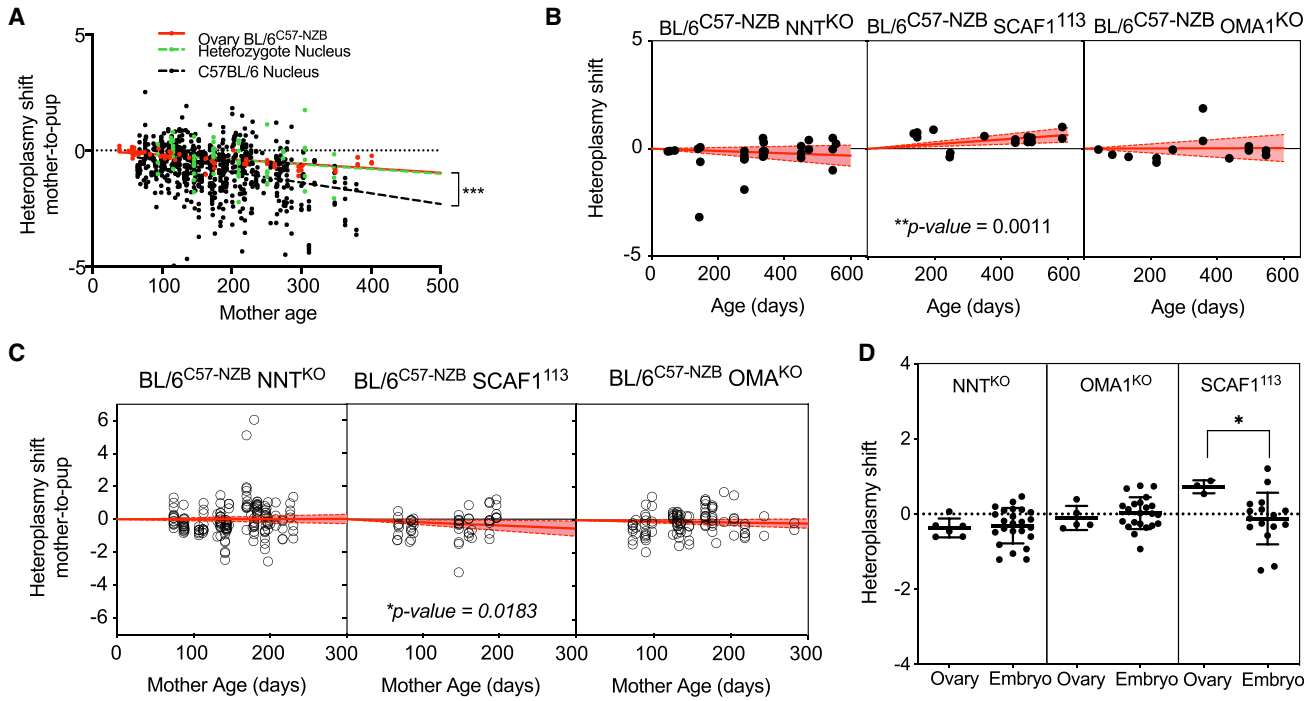

Figure 4. MtDNA Haplotype Competition in Oocyte Biogenesis and Embryo Development Are Determined by Nuclear Context

(A) Mother-to-pup heteroplasmic shift in the inbred (homozygote) C57BL/6 nuclear background (data from Figure 1C), compared with the F1 of BL/6$^{C57\text{-}NZB}$ females with NZB^{NZB} males to generate a non-inbred (heterozygote) background. Each dot corresponds to a different individual.

(B) Evaluation of ovary heteroplasmy with the age of the mother in heteroplasmic females with alterations in the indicated nuclear genes with respect to the original heteroplasmic animal (see Figure 1A). Each dot represents the heteroplasmy shift of the ovary from a different female.

(C) Comparative behavior of the mother-to-pup heteroplasmic shift with the age of the mother in heteroplasmic strains, with alterations in the indicated nuclear genes. Each dot corresponds to a different individual.

(A–C) Significant non-zero slope, linear regression, *$p < 0.05$, **$p < 0.01$, ***$p < 0.001$.

(D) Heteroplasmy development between pluripotent classes 0 (ovary) and III (5.5–6.5 dpc embryos) in heteroplasmic lines with alterations in the indicated nuclear genes (mean ± SD, two-tailed t test, *$p < 0.05$). Eye and tail were used as the reference tissues to calculate the heteroplasmy shift.

Embryonic mtDNA Segregation Is Determined by Nuclear-Mitochondrial Interaction

All the studies on mtDNA segregation performed in mouse models use inbred strains that are homozygotic for most of their nuclear genes. This situation is rather unnatural: in every generation, maternally transmitted mtDNA is confronted with new nuclear alleles that offer novel variability in nuclear-encoded mitochondrial genes from the father. To translate our observations into a more realistic situation, we bred heteroplasmic females with NZB/OlaHsd males to induce heterozygosity in the first generation of heteroplasmic animals. Strikingly, the induction of heterozygosity markedly reduces the observed embryonic selection toward C57 mtDNA (Figure 4A).

To investigate the mechanism behind this mito-nuclear interaction, we next focused on specific genes known to mildly influence mitochondrial performance that can differ between NZB/OlaHsd and C57BL/6 strains: supercomplex assembly factor 1 (SCAF1 or Cox7a2l) and the nicotinamide nucleotide transhydrogenase (NNT). SCAF1 is required for the superassembly between complexes III and IV of the mitochondrial electron transport chain (Cogliati et al., 2016), and it is mutated in all C57BL/6 sub-strains, which have lost this capacity without major effects on health or fertility (Lapuente-Brun et al., 2013). NNT is an integral mitochondrial inner membrane enzyme that couples the hydride transfer between NAD(H) and NADP(+) to proton translocation across the inner membrane to produce NADPH in the mitochondrial matrix. NNT is needed for biosynthetic processes and free radical detoxification. The C57BL/6J sub-strain naturally lacks functional NNT. Despite this, the animals are healthy and fertile but lose versatility in the proper adaptation of OXPHOS to environmental changes and may develop some minor impairments (Picard et al., 2015). The NZB/OlaHsd strains harbor the wild-type version of both genes, while our heteroplasmic animals harbor the mutant version of SCAF1 and the wild-type version of the NNT. Finally, we also considered nuclear factors controlling mitochondrial dynamics. Mitochondrial fission is related to autophagy and removal of mitochondria via mitophagy and hence can shape the genetic structure of cellular mtDNA populations (Shirihai et al., 2015). Tissue-specific response to mtDNA segregation in heteroplasmic mice with mutated dynamin-related protein 1 (DRP) involved in mitochondrial fission has been reported (Jokinen et al., 2016). Other fusion proteins (i.e., MFN1, MFN2, and OPA1) may play a crucial role in mtDNA nucleoids segregation (Carelli et al., 2015). It is possible that functional variations in these (and/or other) genes could impact mitochondrial function and influence mtDNA segregation during germline transmission.

To explore the interplay between these processes and mtDNA population structure, we generated three novel heteroplasmic mouse models to assess the relative relevance for mtDNA segregation of (1) the relevance of ROS signaling/detoxification (NNT^{KO} mice), (2) the role of the superassembly of the respiratory complexes ($SCAF1^{113}$ mice), or (3) the mechanism of fragmentation and removal of damaged mitochondria under stress ($OMA1^{KO}$ mice).

First, we evaluated whether variability in these nuclear genes impacts on the previously observed segregation of mtDNA in ovary with the age of the mother. Comparison between each genotype with the control heteroplasmic group showed that the three different nuclear modifications alter the original segregation toward C57 mtDNA in ovaries with age (compare Figure 1A with Figure 4B). Thus, $BL/6^{C57\text{-}NZB}$:NNT^{KO} and $BL/6^{C57\text{-}NZB}$:$OMA1^{KO}$ showed no segregation preference, while $BL/6^{C57\text{-}NZB}$:$SCAF1^{113}$ shifted their preference from C57 toward NZB mtDNA. Next, we evaluated if variability in these nuclear genes impacts the mother-to-pup transmission of heteroplasmy. For that, tail heteroplasmic levels of the mothers from different strains were measured at the time of weaning. In agreement with the lack of preferences in ovary (Figure 4B), the ablation of NNT or OMA1 erased the preference toward C57 mtDNA during mother-to-pup transmission observed in the control heteroplasmic animals (compare Figure 1C with Figure 4C). Surprisingly, the tendency to favor NZB in ovaries induced by the re-expression of SCAF1 was fully reverted in mother-to-pup transmission, which again showed a preference in favor of C57 mtDNA (Figure 4C). The coherence between the lack of preferential segregation in ovary and mother-to-pup strongly suggests that the observed phenomenon of embryonic segregation was also lost when NNT or OMA1 genes are ablated. In fact, no changes in the heteroplasmic proportions between ovary and 6.5 dpc embryos could be detected (Figure 4D).

On the other hand, the change in preferred mtDNA in ovary (NZB instead of C57) in mother-to-pup shown in $SCAF1^{113}$ animals predicts that the embryo-stage segregation in favor of C57 mtDNA should be strong. In agreement with this prediction, we found that the heteroplasmic proportion between mother ovary and 6.5 days embryos in $SCAF^{113}$ animals experiences a drastic shift toward C57 mtDNA haplotype, indicative of a strong mtDNA selection during early embryo development.

DISCUSSION

We have shown here that intergenerational wild-type mtDNA haplotype selection is common and depends on the impact of the mtDNA haplotype on the performance of the OXPHOS system. We described that in addition to the mtDNA selection during female germline maturation, a second step of mtDNA selection happened at early embryonic stages. Fuel preference, mitochondrial dynamics regulation, and differential mitochondrial ROS handling all play a substantial role in the driving force of the selection. This dependence helps to resolve one of the historic debates on the topic of mtDNA selection: under a variety of different circumstances, which we reveal and quantify, different degrees of mtDNA selection (including none) may be observed. Together, these observations reflect that the communication between mtDNA and the nuclear genome determines the dynamics of cellular mtDNA populations: selection of one or other of the haplotypes or no selection at all. Our data provide an explanation for apparently conflicting conclusions resulting from the diverse nuclear genotypes of the inbred mouse strains used (Jenuth et al., 1996; Sharpley et al., 2012).

If wild-type mtDNA haplotype variability can cause sufficient functional differences to trigger segregation, it is expected that overtly pathological haplotypes would exert a stronger impact. In this sense, the only two available examples in mice concluded that pathological mutations are selectively eliminated through germline transmission (Fan et al., 2008; Stewart et al., 2008). In both mouse models a similar, but not identical, nuclear background was used. The report from Wallace's laboratory (Fan et al., 2008) used mouse female ESC line CC9.3.1 isolated from 129SvEv-Gpilc embryo (129 mice are wild type for NNT and $SCAF1^{113}$). ESCs harboring the mutant mtDNA were injected in C57BL/6NHsd female blastocysts and transferred into pseudopregnant females. After that, female chimeras were identified and mated with C57BL6/J males (NNT^{KO}, $SCAF1^{111}$). Therefore, although the genotype for these two genes is uncertain, they should shift to NNT^{KO}, $SCAF1^{111}$ with subsequent crosses, a genetic context that may enhance mother-to-offspring segregation. Interestingly, they reported that the severe mutation that they followed in heteroplasmy (ND6 frameshift) completely disappears in subsequent litters of the same female and in along two or three generations (Fan et al., 2008). The report from Stewart and coworkers investigated the fate of mtDNA mutations generated in the mtDNA-mutator mice were the functional gamma-pol was restored (Stewart et al., 2008). All the studies were performed in the C57BL/6N background (NNT^{WT} and $SCAF1^{111}$) the nuclear context in which we found the more efficient segregation between mother-to-offspring mtDNA transmission. It is in this context where Stewart and co-workers found a very strong selection against missense mutations.

In contrast to the studies in mice, selective elimination of the defective mtDNA in humans does not always operate. An array of behaviors from random drift to positive or negative selection for the mutated mtDNA was documented (Otten et al., 2018). We propose that differences in nuclear background may be responsible for this discrepancy between mice and humans and that further studies in mouse models should be performed to evaluate this issue.

The relationship between mitochondrial ROS and heteroplasmy has been previously highlighted (Hämäläinen et al., 2013). Thus, elevated levels of H_2O_2 production by mitochondria caused by elevated mtDNA mutagenesis, disrupted cellular redox signaling and, as a consequence of that, reduced pluripotent stem cell reprogramming efficiency and self-renewal capacity (Hämäläinen et al., 2015). On the other hand, iPSC generation from human patients harboring elevated levels of the 3,243 common MELAS mutation induced a drastic selective response against heteroplasmy (Hämäläinen et al., 2013). Both observations are consistent with those reported here and reinforce the relevance of mitochondrial mediated ROS signaling and its sensitivity to mtDNA variations or mutations. Thus, the use of antioxidants (NAC) or a genetic nuclear background were mitochondrial ROS handling is impaired (lack of NNT), obliterate the specific ROS signal that drives the differentiation between NZB and C57 mtDNA haplotypes. In the same line of thought,

part of the effects induced by the recovery of the wild-type version of SCAF1 may be related to its effects in ROS handling, although it has also implication in the adaptation to cell stress (Balsa et al., 2019). The improved understanding of the molecular link between ROS and mtDNA haplotype selection may open an unexplored way to prevent the transmission of mtDNA-linked diseases. By the same token, understanding how mitochondrial quality control and the regulation of OXPHOS dynamics is transduced into the molecular mechanisms that drive non-random mtDNA segregation will open the possibility to prevent the maternal transmission of mtDNA-linked diseases.

Mitochondria from the sperm enter the oocyte upon fertilization (Cummins, 2000). Two concurrent mechanism guarantee uniparental transmission, the active elimination of the paternal mitochondria (Sato and Sato, 2011; Zhou et al., 2016) and the enormous dilution of the paternal mtDNA (~100 copies among ~200,000 copies). The mechanism of elimination of the sperm mitochondria may "leak," generating heteroplasmy in mammals (Gyllensten et al., 1991; Zhao et al., 2004), flies (Dokianakis and Ladoukakis, 2014), and also in humans (Luo et al., 2018; Schwartz and Vissing, 2002), but these are considered very rare cases. However, this possibility, together with the potential artificial generation of mtDNA heteroplasmy by novel medical technologies, highlights the relevance to understand the implications and dynamics of confronting different pairs of human mtDNA variants.

Limitations of Study

Our study assessed the behavior of two defined mtDNA haplotypes under one homozygote nuclear genetic background. The question of at which extension our observations can be considered frequent within the mtDNA and nDNA genetic context in mammals in general and in humans in particular, may require further confirmation. In this sense, a very recent publication from the group of Chinnery in Cambridge, UK, documented the existence of selective segregation of mtDNA in the human germline driven by the nuclear background. They found that this impact is so strong that it can be observed in just one generation (Wei et al., 2019). Therefore, in accordance with this report, the observed nDNA/mtDNA interaction may not be a peculiarity of a given genetic context in mice (C57BL/6) but a general phenomenon occurring also in human populations.

STAR★METHODS

Detailed methods are provided in the online version of this paper and include the following:

SUPPLEMENTAL INFORMATION

Supplemental Information can be found online at https://doi.org/10.1016/j.cmet.2019.09.007.

ACKNOWLEDGMENTS

We thank Dr. C. López-Otin for the OMA1^{KO} mice; Dra. R. Martínez-de-Mena, I. Martinez-Carrascoso, M.M. Muñoz-Hernandez, A. Gonzalez-Guerra, E.R. Martínez-Jiménez, and Dr. Concepción Jimenez for technical assistance; M. Cueva and R. Álvarez for mouse work; and A. Molina-Iracheta and R. Doohan for histology. A.V.L.-V. was supported by fellowship SVP-2013-068089 from MCIU. I.G.J. thanks ERC StG EvoConBiO, and a Turing fellowship from the Alan Turing Institute. N.J. thanks EP/N014529/1. SAF2017-84494-C2-R and Programa Red Guipuzcoana de Ciencia, Tecnología e Información 2018-CIEN-000058-01, and the Basque Government under its ELKARTEK research program (ref: KK-2019/00015) to J.R.-C. The work at CIC biomaGUNE was performed under the Maria de Maeztu Units of Excellence Program from the Spanish State Research Agency – Grant No. MDM-2017-0720. This study was supported by grants from the MCNU (SAF2015-65633-R), the EU (UE0/MCA317433), the Biomedical Research Networking Center on Frailty and Healthy Ageing (CIBERFES-ISCiii), and the HFSP agency (RGP0016/2018) to J.A.E. The CNIC is supported by the Instituto de Salud Carlos III (ISCIII), the Ministerio de Ciencia, Innovación y Universidades (MCNU), and the Pro CNIC Foundation, and is a Severo Ochoa Center of Excellence (SEV-2015-0505).

AUTHOR CONTRIBUTIONS

A.L.-P. and A.V.L.-V. performed most of the mouse and experimental work with the help of R.J.-M. I.G.J. and N.S.J. performed the data analysis and mathematical modeling. J.M.F.-T. and L.M.C. generated the heteroplasmic animals. A.V.L.-V., J.P., and J.R.-C. performed and analyzed the *in vivo* imaging data. J.L. provided the radiotracers. R.H.H. and A.S. contributed to the generation and analysis of the iPSC and commented on the manuscript. A.G., C.C., R.S., and M.T. contributed to the embryo manipulation and analysis. J.A.E., A.L.-P., and A.V.L.-V. participated in the design of the experimental work, the integrated analysis of the results, and the writing of the manuscript. J.A.E. directed and designed the research.

DECLARATION OF INTERESTS

The authors declare no competing interests.

Received: January 22, 2019
Revised: June 12, 2019
Accepted: September 10, 2019
Published: October 3, 2019

REFERENCES

Balsa, E., Soustek, M.S., Thomas, A., Cogliati, S., García-Poyatos, C., Martín-García, E., Jedrychowski, M., Gygi, S.P., Enriquez, J.A., and Puigserver, P.

(2019). ER and nutrient stress promote assembly of respiratory chain supercomplexes through the PERK-eIF2α axis. Mol. Cell *74*, 877–890.e6.

Burgstaller, J.P., Johnston, I.G., Jones, N.S., Albrechtová, J., Kolbe, T., Vogl, C., Futschik, A., Mayrhofer, C., Klein, D., Sabitzer, S., et al. (2014). MtDNA segregation in heteroplasmic tissues is common in vivo and modulated by haplotype differences and developmental stage. Cell Rep. *7*, 2031–2041.

Burgstaller, J.P., Kolbe, T., Havlicek, V., Hembach, S., Poulton, J., Piálek, J., Steinborn, R., Rülicke, T., Brem, G., Jones, N.S., et al. (2018). Large-scale genetic analysis reveals mammalian mtDNA heteroplasmy dynamics and variance increase through lifetimes and generations. Nat. Commun. *9*, 2488.

Carelli, V., Maresca, A., Caporali, L., Trifunov, S., Zanna, C., and Rugolo, M. (2015). Mitochondria: biogenesis and mitophagy balance in segregation and clonal expansion of mitochondrial DNA mutations. Int. J. Biochem. Cell Biol. *63*, 21–24.

Cogliati, S., Calvo, E., Loureiro, M., Guaras, A.M., Nieto-Arellano, R., Garcia-Poyatos, C., Ezkurdia, I., Mercader, N., Vázquez, J., and Enriquez, J.A. (2016). Mechanism of super-assembly of respiratory complexes III and IV. Nature *539*, 579–582.

Corroyer-Dulmont, A., Chakhoyan, A., Collet, S., Durand, L., MacKenzie, E.T., Petit, E., Bernaudin, M., Touzani, O., and Valable, S. (2015). Imaging modalities to assess oxygen status in glioblastoma. Front. Med. (Lausanne) *2*, 57.

Craven, L., Tuppen, H.A., Greggains, G.D., Harbottle, S.J., Murphy, J.L., Cree, L.M., Murdoch, A.P., Chinnery, P.F., Taylor, R.W., Lightowlers, R.N., et al. (2010). Pronuclear transfer in human embryos to prevent transmission of mitochondrial DNA disease. Nature *465*, 82–85.

Cuezva, J.M., Chen, G., Alonso, A.M., Isidoro, A., Misek, D.E., Hanash, S.M., and Beer, D.G. (2004). The bioenergetic signature of lung adenocarcinomas is a molecular marker of cancer diagnosis and prognosis. Carcinogenesis *25*, 1157–1163.

Cummins, J.M. (2000). Fertilization and elimination of the paternal mitochondrial genome. Hum. Reprod. *15*, 92–101.

Díez-Sánchez, C., Ruiz-Pesini, E., Montoya, J., Pérez-Martos, A., Enríquez, J.A., and López-Pérez, M.J. (2003). Mitochondria from ejaculated human spermatozoa do not synthesize proteins. FEBS Lett. *553*, 205–208.

Dokianakis, E., and Ladoukakis, E.D. (2014). Different degree of paternal mtDNA leakage between male and female progeny in interspecific Drosophila crosses. Ecol. Evol. *4*, 2633–2641.

Fan, W., Waymire, K.G., Narula, N., Li, P., Rocher, C., Coskun, P.E., Vannan, M.A., Narula, J., Macgregor, G.R., and Wallace, D.C. (2008). A mouse model of mitochondrial disease reveals germline selection against severe mtDNA mutations. Science *319*, 958–962.

Grimes, D.R., Warren, D.R., and Warren, S. (2017). Hypoxia imaging and radiotherapy: bridging the resolution gap. Br. J. Radiol. *90*, 20160939.

Guarás, A., Perales-Clemente, E., Calvo, E., Acín-Peréz, R., Loureiro-Lopez, M., Pujol, C., Martínez-Carrascoso, I., Nuñez, E., García-Marqués, F., Rodríguez-Hernández, M.A., et al. (2016). The CoQH2/CoQ ratio serves as a sensor of respiratory chain efficiency. Cell Rep. *15*, 197–209.

Gyllensten, U., Wharton, D., Josefsson, A., and Wilson, A.C. (1991). Paternal inheritance of mitochondrial DNA in mice. Nature *352*, 255–257.

Hämäläinen, R.H., Manninen, T., Koivumäki, H., Kislin, M., Otonkoski, T., and Suomalainen, A. (2013). Tissue- and cell-type-specific manifestations of heteroplasmic mtDNA 3243A>G mutation in human induced pluripotent stem cell-derived disease model. Proc. Natl. Acad. Sci. U S A *110*, E3622–E3630.

Hämäläinen, R.H., Ahlqvist, K.J., Ellonen, P., Lepistö, M., Logan, A., Otonkoski, T., Murphy, M.P., and Suomalainen, A. (2015). mtDNA mutagenesis disrupts pluripotent stem cell function by altering redox signaling. Cell Rep. *11*, 1614–1624.

Jenuth, J.P., Peterson, A.C., Fu, K., and Shoubridge, E.A. (1996). Random genetic drift in the female germline explains the rapid segregation of mammalian mitochondrial DNA. Nat. Genet. *14*, 146–151.

Johnston, I.G., Burgstaller, J.P., Havlicek, V., Kolbe, T., Rülicke, T., Brem, G., Poulton, J., and Jones, N.S. (2015). Stochastic modelling, Bayesian inference, and new in vivo measurements elucidate the debated mtDNA bottleneck mechanism. eLife *4*, e07464.

Johnston, I.G., and Jones, N.S. (2016). Evolution of cell-to-cell variability in stochastic, controlled, heteroplasmic mtDNA populations. Am. J. Hum. Genet. *99*, 1150–1162.

Johnston, I.G., Gaal, B., Neves, R.P.D., Enver, T., Iborra, F.J., and Jones, N.S. (2012). Mitochondrial variability as a source of extrinsic cellular noise. PLoS Comput. Biol. *8*, e1002416.

Jokinen, R., Marttinen, P., Stewart, J.B., Neil Dear, T., and Battersby, B.J. (2016). Tissue-specific modulation of mitochondrial DNA segregation by a defect in mitochondrial division. Hum. Mol. Genet. *25*, 706–714.

Kang, E., Wu, J., Gutierrez, N.M., Koski, A., Tippner-Hedges, R., Agaronyan, K., Platero-Luengo, A., Martinez-Redondo, P., Ma, H., Lee, Y., et al. (2016). Mitochondrial replacement in human oocytes carrying pathogenic mitochondrial DNA mutations. Nature *540*, 270–275.

Lapuente-Brun, E., Moreno-Loshuertos, R., Acín-Pérez, R., Latorre-Pellicer, A., Colás, C., Balsa, E., Perales-Clemente, E., Quirós, P.M., Calvo, E., Rodríguez-Hernández, M.A., et al. (2013). Supercomplex assembly determines electron flux in the mitochondrial electron transport chain. Science *340*, 1567–1570.

Latorre-Pellicer, A., Moreno-Loshuertos, R., Lechuga-Vieco, A.V., Sánchez-Cabo, F., Torroja, C., Acín-Pérez, R., Calvo, E., Aix, E., González-Guerra, A., Logan, A., et al. (2016). Mitochondrial and nuclear DNA matching shapes metabolism and healthy ageing. Nature *535*, 561–565.

Lee, H.S., Ma, H., Juanes, R.C., Tachibana, M., Sparman, M., Woodward, J., Ramsey, C., Xu, J., Kang, E.J., Amato, P., et al. (2012). Rapid mitochondrial DNA segregation in primate preimplantation embryos precedes somatic and germline bottleneck. Cell Rep. *1*, 506–515.

Luo, S., Valencia, C.A., Zhang, J., Lee, N.C., Slone, J., Gui, B., Wang, X., Li, Z., Dell, S., Brown, J., et al. (2018). Biparental inheritance of mitochondrial DNA in humans. Proc. Natl. Acad. Sci. U S A *115*, 13039–13044.

Moreno-Loshuertos, R., Acín-Peréz, R., Fernández-Silva, P., Movilla, N., Pérez-Martos, A., Rodríguez de Córdoba, S., Gallardo, M.E., and Enríquez, J.A. (2006). Differences in reactive oxygen species production explain the phenotypes associated with common mouse mitochondrial DNA variants. Nat. Genet. *38*, 1261–1268.

Otten, A.B.C., Sallevelt, S.C.E.H., Carling, P.J., Dreesen, J.C.F.M., Drüsedau, M., Spierts, S., Paulussen, A.D.C., de Die-Smulders, C.E.M., Herbert, M., Chinnery, P.F., et al. (2018). Mutation-specific effects in germline transmission of pathogenic mtDNA variants. Hum. Reprod. *33*, 1331–1341.

Picard, M., McManus, M.J., Gray, J.D., Nasca, C., Moffat, C., Kopinski, P.K., Seifert, E.L., McEwen, B.S., and Wallace, D.C. (2015). Mitochondrial functions modulate neuroendocrine, metabolic, inflammatory, and transcriptional responses to acute psychological stress. Proc. Natl. Acad. Sci. U S A *112*, E6614–E6623.

Pikó, L., and Taylor, K.D. (1987). Amounts of mitochondrial DNA and abundance of some mitochondrial gene transcripts in early mouse embryos. Dev. Biol. *123*, 364–374.

Quirós, P.M., Ramsay, A.J., Sala, D., Fernández-Vizarra, E., Rodríguez, F., Peinado, J.R., Fernández-García, M.S., Vega, J.A., Enríquez, J.A., Zorzano, A., et al. (2012). Loss of mitochondrial protease OMA1 alters processing of the GTPase OPA1 and causes obesity and defective thermogenesis in mice. EMBO J. *31*, 2117–2133.

Ronchi, J.A., Figueira, T.R., Ravagnani, F.G., Oliveira, H.C.F., Vercesi, A.E., and Castilho, R.F. (2013). A spontaneous mutation in the nicotinamide nucleotide transhydrogenase gene of C57BL/6J mice results in mitochondrial redox abnormalities. Free Radic. Biol. Med. *63*, 446–456.

Sato, M., and Sato, K. (2011). Degradation of paternal mitochondria by fertilization-triggered autophagy in C. elegans embryos. Science *334*, 1141–1144.

Schwartz, M., and Vissing, J. (2002). Paternal inheritance of mitochondrial DNA. N. Engl. J. Med. *347*, 576–580.

Sharpley, M.S., Marciniak, C., Eckel-Mahan, K., McManus, M., Crimi, M., Waymire, K., Lin, C.S., Masubuchi, S., Friend, N., Koike, M., et al. (2012). Heteroplasmy of mouse mtDNA is genetically unstable and results in altered behavior and cognition. Cell *151*, 333–343.

Shirihai, O.S., Song, M., and Dorn, G.W. (2015). How mitochondrial dynamism orchestrates mitophagy. Circ. Res. *116*, 1835–1849.

Stewart, J.B., Freyer, C., Elson, J.L., Wredenberg, A., Cansu, Z., Trifunovic, A., and Larsson, N.G. (2008). Strong purifying selection in transmission of mammalian mitochondrial DNA. PLoS Biol. *6*, e10.

Tachibana, M., Sparman, M., Sritanaudomchai, H., Ma, H., Clepper, L., Woodward, J., Li, Y., Ramsey, C., Kolotushkina, O., and Mitalipov, S. (2009). Mitochondrial gene replacement in primate offspring and embryonic stem cells. Nature *461*, 367–372.

Treuting, P.M., Dintzis, S.M., and Montine, K.S. (2017). Comparative Anatomy and Histology (Academic Press).

Wai, T., Teoli, D., and Shoubridge, E.A. (2008). The mitochondrial DNA genetic bottleneck results from replication of a subpopulation of genomes. Nat. Genet. *40*, 1484–1488.

Warren, D.R., and Partridge, M. (2016). The role of necrosis, acute hypoxia and chronic hypoxia in 18F-FMISO PET image contrast: a computational modelling study. Phys. Med. Biol. *61*, 8596–8624.

Wartiovaara, A., and Syvänen, A.C. (2002). Analysis of nucleotide sequence variations by solid-phase minisequencing. Methods Mol. Biol. *187*, 57–63.

Wei, W., Tuna, S., Keogh, M.J., Smith, K.R., Aitman, T.J., Beales, P.L., Bennett, D.L., Gale, D.P., Bitner-Glindzicz, M.A.K., Black, G.C., et al. (2019). Germline selection shapes human mitochondrial DNA diversity. Science *364*, eaau6520.

Wittig, I., Braun, H.P., and Schägger, H. (2006). Blue native PAGE. Nat. Protoc. *1*, 418–428.

Woltjen, K., Hämäläinen, R., Kibschull, M., Mileikovsky, M., and Nagy, A. (2011). Transgene-free production of pluripotent stem cells using piggyBac transposons. Methods Mol. Biol. *767*, 87–103.

Woods, D.C., and Tilly, J.L. (2015). Autologous germline mitochondrial energy transfer (AUGMENT) in human assisted reproduction. Semin. Reprod. Med. *33*, 410–421.

Yamada, M., Emmanuele, V., Sanchez-Quintero, M.J., Sun, B., Lallos, G., Paull, D., Zimmer, M., Pagett, S., Prosser, R.W., Sauer, M.V., et al. (2016). Genetic drift can compromise mitochondrial replacement by nuclear transfer in human oocytes. Cell Stem Cell *18*, 749–754.

Zhao, X., Li, N., Guo, W., Hu, X., Liu, Z., Gong, G., Wang, A., Feng, J., and Wu, C. (2004). Further evidence for paternal inheritance of mitochondrial DNA in the sheep (Ovis aries). Heredity (Edinb) *93*, 399–403.

Zhou, Q., Li, H., Li, H., Nakagawa, A., Lin, J.L.J., Lee, E.S., Harry, B.L., Skeen-Gaar, R.R., Suehiro, Y., William, D., et al. (2016). Mitochondrial endonuclease G mediates breakdown of paternal mitochondria upon fertilization. Science *353*, 394–399.

STAR★METHODS

KEY RESOURCES TABLE

REAGENT or RESOURCE	SOURCE	IDENTIFIER
Antibodies		
NDUFA9	Abcam	Ab14713
COI	Invitrogen	459600
UQCRC2 (Core2)	ProteinTech	14742-I-AP
SDHA	ThermoFisher	459200
GAPDH	Abcam	Ab8245
ATPB	Abcam	Ab14730
Mouse IgG (H+L) DyLight 800	Rockland	610-145-002
Mouse IgG (H+L) Alexa Fluor 680	Invitrogen	A21057
Rabbit IgG (H+L) DyLight 800	Rockland	611-145-122
Chemicals, Peptides, and Recombinant Proteins		
Φ29 DNA polymerase	New England Biolabs	M0269L
BamH1	New England Biolabs	R0136M
SspI	New England Biolabs	R0132S
Lambda Exonuclease.	New England Biolabs	M0262S
T4 DNA ligase	New England Biolabs	M0202M
TMRM	ThermoFisher	T668
H_2DCFDA	ThermoFisher	D399
Digitonin	Sigma-Aldrich	D5628
[^{18}F]-FMISO	This Paper	N/A
[^{18}F]-FDG	This Paper	N/A
N-Acetyl-L-cysteine	Sigma-Aldrich	A7250
Critical Commercial Assays		
kit 5Prime Master Mix	5Prime	2200200
DNeasy Blood &Tissue kit	Qiagen	69506
Dulbecco's modified Eagle's medium	Gibco	41966029
Seahorse XFe96 FluxPaks	Agilent	102416-100
CyQUANT NF Cell Proliferation Assay Kit	ThermoFisher	C35006
PVDF transfer membrane Immobilon-FL	Merck Millipore	IPFL00010
SEA BLOCK Blocking buffer	ThermoFisher	37527
Neon Trasfection System 100μl kit	Invitrogen	MPK10025
Vector Red Alkaline Phosphatase (Red AP) Substrate Kit	Vector Laboratories	SK-5100
Experimental Models: Organisms/Strains		
C57BL/6JOlaHsd	Envigo	N/A
CD1	Charles River Laboratories	N/A
C57BL/6J	The Jackson Laboratories	000664
Oligonucleotides		
Mouse 3862-3884 (Fw) 5'-AAGCTATCGGG CCCATACCCCG-3'	This Paper	N/A
Mouse 4503-4525 (Rv) 5'-GTTGAGTAGAGT GAGGGATGGG-3'	This Paper	N/A
ppC57 probe -P- ATTACTCTCTTCTGG TTCCTTTTACGA CCTCAATGCTGCTGCTGTACTACTCTTC ACAGTGTACA GGTTA -3'	This Paper	N/A

(*Continued on next page*)

Continued		
REAGENT or RESOURCE	SOURCE	IDENTIFIER
ppNZB probe 5'-P- ATTACTCTCTTCTGGCCTTTCC TACGACCTCAATGCACATGTTTGGCTCCTCTTCAC AGTGTACAGGTTC -3'	This Paper	N/A
Lin33 (ppC57) 5'-Cy3-CCTCAATGCTGCTGCTGTACTAC-3'	This Paper	N/A
Lin16 (ppNZB) 5'-FITC-CCTCAATGCACATGTTTGGCTCC-3'; 5'-Cy5-CCTCAATGCACATGTTTGGCTCC-3'	This Paper	N/A
Software and Algorithms		
GraphPad Prism Version 6	GraphPad Software	N/A
ImageJ v.1.6.0	NIH	N/A
NDP view2 Software	Hamamatsu Photonics	U12388-01
FACSDiva Software	BD Biosciences	N/A
FlowJo	FlowJo LLC, BD Biosciences	N/A

LEAD CONTACT AND MATERIALS AVAILABILITY

Request of information and material should be made to José Antonio Enriquez. Mouse and cell lines generated in this study are available upon request for a non-commercial use under a Material Transfer agreement.

EXPERIMENTAL MODEL AND SUBJECT DETAILS

This study used mouse and cellular models which were generated from the animals.

Animal Models

Mice were kept in standard housing conditions in a specific pathogen free (SPF) status facility on a 12-hour light/dark cycle at 20-24°C and relative humidity at 45-65%. The maintenance conditions are checked and registered daily. All animal procedures conformed to EU Directive 86/609/EEC and Recommendation 2007/526/EC regarding the protection of animals used for experimental and other scientific purposes, enforced in Spanish law under RD 1201/2005 and RD 53/2013. Approval of the different experimental protocols requires the estimation of adequate sample sizes as well as the definition of the randomization and blinding criteria. Mice received ad libitum food and water (5K67 LabDiet) and the number of mice per cage is limited and adapted to RD 53/2013. Experiments were carried out with males and females indistinctively, and the details of the age of the mice can be found in the figure legends and results. C57BL/6JOlaHsd and CD-1 wild-type mice were purchased from Envigo and Charles River Laboratories respectively, and the mice with C57BL/6J nuclear background were from The Jackson Laboratory. The conplastic mouse strain with C57BL/6 nuclear genome and the NZB/OlaHsd mtDNA was described before (Latorre-Pellicer et al., 2016). OMA1^{KO} mice on the C57BL/6JOlaHsd background, were generated as described in Quirós et al. (2012). Heteroplasmic mice were generated by electro-fusing cytoplasts from conplastic BL/6^{NZB} zygotes to recipient C57BL/6JOlaHsd (BL/6^{C57}) one-cell embryos, cultured overnight and transplanted as two-cell embryos into pseudo pregnant Hsd:ICR (CD-1) females to complete development to term as previously described (Jenuth et al., 1996). To the best of our knowledge, no consensus rule to name heteroplasmic mouse strains exists. Here, we propose the following designation to name heteroplasmic mouse strains: NUCLEAR GENOME- - mtCYTOPLASMIC GENOME #1 + CYTOPLASMIC GENOME #2 [i.e., C57BL/6-mtC57BL/6+NZB, a strain with the nuclear genome of C57BL/6JOlaHsd and the cytoplasmic (mitochondrial) genome of C57BL/6JOlaHsd and NZB/B1NJ]. For simplicity, we label this BL/6$^{C57\text{-}NZB}$ throughout this report. Heteroplasmic females (BL/6$^{C57\text{-}NZB}$) were outcrossed with males BL/6^{C57}. Only females with an initial level of mtDNA NZB heteroplasmy above 20% were used for colony maintenance. To produce heteroplasmic mice OMA1^{KO}, BL/6$^{C57\text{-}NZB}$ female were outcrossed to male OMA1^{KO} (C57BL/6JOlaHsd background) to generate an F1 heterozygote mice, which were then intercrossed to obtain a F2 OMA1^{KO} heteroplasmic mice. *Oma1* was genotyped as described (Quirós et al., 2012). To produce heteroplasmic mice NNT^{KO}, BL/6$^{C57\text{-}NZB}$ females were outcrossed with NNT^{KO} males (C57BL/6J background) to generate the F1 heterozygote mice, which were then intercrossed to obtain the F2 NNT^{KO} heteroplasmic mice. Heteroplasmic strains were maintained by outcrossing heteroplasmic females (BL/6$^{C57\text{-}NZB}$ NNT^{KO}) with BL/6^{C57} NNT^{KO} males. *Nnt* was genotyped as described in Ronchi et al. (2013). To produce heteroplasmic mice SCAF1^{113}, BL/6$^{C57\text{-}NZB}$ females were outcrossed to SCAF1^{113} males (C57BL/6JOlaHsd nuclear background) to generate the F1 heterozygote mice, which were then intercrossed to obtain the F2 SCAF1^{113} heteroplasmic mice. Heteroplasmic strains were maintained by outcrossing heteroplasmic females (BL/6$^{C57\text{-}NZB}$ SCAF1^{113}) with BL/6^{C57} SCAF1^{113} males. *Scaf1* was genotyped as described in Cogliati et al. (2016).

Cellular Models

Mouse embryo fibroblast (MEF) cell lines were isolated from 13.5 dpc from both sexes of embryos using standard protocol. Each embryo was dissected into 10ml of sterile PBS, voided of its internal organs, head, and legs. After 30 min incubation with gentle shaking at 37°C with 5ml 0,1% trypsin, cells were plated in two 100 mm dishes and incubated for 24-48h. All MEFs used for iPSCs studies were within the first three passages. To establish the immortalized MEF lines, early passage MEFs were seeded in 60 mm plates and infected with 10^5 IU/ml packaged retrovirus E6/E7. Selection was performed with 400 μg/ml of G418 during 10 days. IPSCs were generated using transposon-mediated gene transfer (Woltjen et al., 2011). The transfections were done using a Neon electroporator (Invitrogen; one pulse; 30 mS; 1,300 V) and Neon Trasfection System 100μl kit (Invitrogen) with 2 μg of DNA and 2.5 x 10^5 cells per electroporation. The culture media was supplemented with 1.5 μg/ml of doxycycline on the next day. For reprogramming in different oxygen tensions, electroporations were split into two separate plates: one cultured in 4% O_2 (Biospherix ExVivo chamber) and the other cultured in a standard room-air incubator of around 21% O_2. For reprogramming in different medium conditions in 21% O_2, the electroporations were split into two separate plates: one cultured with standard medium, and the other supplemented with 1 mM NAC (Sigma). To assess the reprogramming efficiency, plates were stained on day 14 for alkaline phosphatase (AP) activity (Vector Red Alkaline Phosphate substrate kit). The relative reprograming efficiency was defined as the proportion of number of iPSC clones generated from identical MEFs number, compared to a reference of 100 defined as the proportion obtained with $BL/6^{C57}$ MEFs under 21% Oxygen concentration.

METHOD DETAILS

Molecular Confirmation and Quantification of Heteroplasmy

To determine the heteroplasmy levels of each tissue or cell culture, total genomic DNA was isolated using DNeasy Blood &Tissue kit (Qiagen). The polymorphic G4276A nucleotide was used to genotype individual animals and tissues. This polymorphism in C57 mtDNA forms part of a BamH1 restriction site, which is absent in NZB mtDNA. Total genomic DNA was PCR amplified using standard conditions with the kit 5Prime Master Mix (5Prime) and the following primers: 5'-AAGCTATCGGGCCCATACCCCG-3' (3862-3884) and 5'-GTTGAGTAGAGTGAGGGATGGG-3' (4503-4525), as follow: 95°C, 30s; 58°C, 30s; 72°C, 45s for 30 cycles. A 15 μl aliquot of PCR was digested with 20 units of BamH1 (New England Biolabs), at 37°C for 2 hours. After agarose gel electrophoresis, DNA was visualized using the Gel Doc XR+System (Bio-Rad), and band intensities were quantified with Quantity One 1-D Analysis Software. The proportion of C57 mtDNA was calculated by adding the intensities of the 414bp and 250bp BamH1-digested fragments and was divided by the sum of the intensities of the undigested 664bp fragments and the 414bp and 250bp BamH1-digested fragments. We monitored it by PCR amplification followed by BamHI digestion to differentiate the two mtDNAs (C57 uncut, NZB cut). normal room air of around 21% O_2 To correct for potential bias in the estimation of the heteroplasmy, we used standard curves generated by mixing pure mutant and wildtype DNAs. We confirm the accuracy of our heteroplasmy estimation by PCR and solid-phase minisequencing (Wartiovaara and Syvänen, 2002).

Padlock Probes

Cells were seeded in Superfrost plus slides (Thermo Scientific) using complete DMEM media lacking phenol-red (10% FBS, 290 μg/mL L-glutamine, 50 μg/mL uridine, 5 mM glucose) and allowed to attach. When the cells reached 80% of confluency they were fixed in 4% (w/v) paraformaldehyde (Sigma) in DMEM media for 15 minutes at 37°C. Cell permeabilization was performed using 95% EtOH and 5% acetic acid for 10 minutes at RT. Slides were then washed with PBS. Enzymatic target preparation was performed with SspI (New Engalnd Biolabs R0132S) for 30 minutes at 37°C. Two washes were done with Buffer A (0.1M Tris-HCl pH 7.5, 0.15 M NaCl and 0.05% Tween-20). 0.2 U/μL of Lambda-exonuclease (New England Biolabs M0262S) was used for 15 minutes at 37°C adding 10% glycerol to the corresponding enzyme buffer. The slides were washed twice with Buffer A. Oligonucleotide sequences were designed (Table S2). Padlock probes (ppC57 and ppNZB) were incubated in a specific hybridization buffer (2X saline-sodium citrate (SSC) buffer, 20% formamide, 0.5 μg/μL salmon sperm DNA) for 15 minutes at 37°C. To remove excess probe, Buffer B was used (2X SSC, 0.05% Tween-20) for 5 minutes at 37°C. DNA padlock probes were circularized by T4 DNA ligase (New England Biolabs M0202M) for 15 minutes at 42°C in Buffer B supplemented with 20% formamide and 1 mM EDTA. Slides were then washed in Buffer A and dehydrated in ethanol. RCA was performed using 1U/ μL of Φ29 DNA polymerase (New England Biolabs M0269L) for 1 hour at 37°C in a shaking platform. Slides were washed three times with Buffer A and Lin16 and Lin33 fluorescence-labelled oligonucleotide (100 nM) hybridization was performed in the hybridization buffer for 30 minutes at 37°C. Slides were then washed with Buffer A followed by PBS-0.01% Tween-20 and dehydrated in ethanol. Vectashield with DAPI mounting media were used for nuclei staining. Specificity of the probes and staining were confirmed by using homoplasmic cell cultures (100% NZB and 100% C57 mtDNA). Leica SP5 confocal and ImageJ v.1.6.0 software was used for image acquisition and data analysis respectively.

Oocyte Collection

Heteroplasmic female mice were superovulated by intraperitoneal administration of 5 IU PMSG (Sigma) to stimulate follicle growth. A single intraperitoneal injection of 5 IU hCG (Sigma) was followed 48 hr later. 16 hr after the hCG injection, mice were euthanized by cervical dislocation and the oviducts dissected out. Ovulated oocytes were collected from the ampullae of the oviducts and placed individually in a 0,2ml sterile tube for genotyping. Ovaries were collected to quantify heteroplasmy.

Embryo Collection

Heteroplasmic females were mated with BL/6^{C57} males. The presence of a vaginal plug was taken as evidence of pregnancy, and 2.5, 5.5, 6.5, 13.5 and 17.5 dpc embryos were collected for genotyping. When indicated, females were treated with 1% NAC in drinking water since vaginal plug was detected.

Sperm Collection

Male mice that had not been mated for more than 2 weeks were euthanized and sperm was collected from the epididymis.

In Vitro mtDNA Segregation Studies

Immortalized MEFS were grown in Dulbecco's modified Eagle's medium (DMEM; Gibco without glucose) supplemented with 10% fetal bovine serum (FBS; Sigma), 1% Penicillin-Streptomycin (Lonza) and 1mM sodium pyruvate (Sigma). Where indicated, the carbon source was: 4.5g/l of glucose (Sigma), 0.9g/l of glucose or 0.9g/l of galactose (Sigma).

SeaHorse Analysis

Oxygen consumption was measured using the XF96 MitoStress Test (Seahorse Bioscience). Oxygen consumption rates were normalized to cell number using CyQuant (ThermoFisher Scientific).

Histological Analysis of the Ovary

Ovaries were collected from homoplasmic and heteroplasmic females, fixed with 4% PFA for 24 hours and sectioned at 5 μm. Four sections from each ovary at three different levels of the tissue (40 μm between each section was discarded) were processed, mounted on a glass slide, stained with H&E and digitalized using NDP view2 Software. Ovaries from females of 3, 6, 9, and 12 months of age were analyzed using ImageJ v.1.6.0 Software (NIH) to assess the percentage of lipofuscin in ovaries. Classification of primordial follicle, primary follicle and growing follicle was done according to Treuting P. and Dintzis S (Treuting et al., 2017).

Mitochondrial Membrane Potential (MMP) and ROS Assessment in MEFs

ROS and MMP were measured in MEFs using 2′-7′dichlorofluorescein diacetate (H_2DCFDA, ThermoFisher, 0.4μM final concentration), and tetramethylrhodamine methyl ester perchlorate (TMRM, Sigma, 100 nM final concentration). A total of 10.000 events were recorded for each sample using the FACSCanto II system (BD Biosciences). All experiments were performed in triplicate. Samples were analyzed with BD FACSDiva Software and an average of the means and standard deviations were calculated using FlowJo Software (v10).

Blue Native Gel Electrophoresis

Supercomplex levels and compositions were analyzed in isolated mitochondria from 12.5 dpc embryos using blue native electrophoresis (BNE) as described previously (Wittig et al., 2006). Mitochondrial proteins were solubilized with 10% digitonin (4g/g) (Sigma D5628) and run on a 3%–13% gradient gel. The gradient gel was prepared in 1.5 mm glass plates using a gradient former connected to a peristaltic pump. Proteins were electroblotted onto PVDF transfer membrane (Immobilon-FL, 0.45 μm, Merck millipore, IPFL00010) for 1 h at 100 V in transfer buffer (48 mM Tris, 39 mM glycine, 20 % EtOH). A Mini Trans- Blot Cell system (BioRad) was used. SEA BLOCK Blocking buffer (ThermoFisher 37527) or PBS with 5 % BSA was used for 1 hour at room temperature (RT) to avoid non-specific binding of antibodies. For protein detection, antibodies were incubated with the membrane for 2 hours at RT. Secondary antibodies were incubated for 45 minutes at RT. The membrane was washed with PBS 0.1 % Tween-20 for 5 minutes three times between primary and secondary antibodies and after secondary antibodies. To study supercomplex assembly, the PVDF membrane was sequentially probed with antibodies against Complex I (anti-NDUFA9), Complex III (anti-UQCRC2), Complex IV (anti-COI), Complex V (anti-ATPB) and Complex II (anti-SDHA) (Table S1).

Western Blot

Proteins in whole embryo lysates were separated using SDS/PAGE and transferred to PVDF membranes (Immobilon-FL, 0.45 μm, Merck millipore, IPFL00010), which were then blocked with 5% (vol/vol) BSA in 0.1 % Tween 20 in PBS for 1 h at room temperature. The membranes were then probed using anti-GAPDH (mouse monoclonal, Abcam, Ab8245), and anti-ATPB (mouse monoclonal Abcam, Ab14730). The secondary antibody was anti-mouse dylight 800 (Rockland, 610145002) and the images were acquired using the ODYSSEY Infrared Imaging System (LI-COR). Protein quantification was performed using ImageJ v.1.6.0 software.

PET-CT in Embryos

In vivo positron emission tomography–computed tomography (PET/CT) imaging was performed with a nanoPET/CT small-animal imaging system (Mediso Medical Imaging Systems, Budapest, Hungary). List-mode PET data acquisition commenced 30 min post intravenous injection of 18 MBq [^{18}F]- FDG or 30 MBq [^{18}F]-fluoromisonidazole ([^{18}F]-FMISO) in 12.5 dpc embryo imaging, and continued for 20 minutes of PET acquisition. At the end of PET acquisitions, scan microCT was performed for attenuation correction and anatomical references. The resulting dynamic PET images were reconstructed in a 105 x 105 matrix (frame rates: 3 x 10 min, 1 x 30 min, 1 x 60 min) using a Tera-Tomo 3D iterative algorithm. Acquisition and reconstruction were performed with proprietary Nucline software (Mediso, Budapest, Hungary) and saved in Dicom format. The images were imported into OsiriX software (Pixmeo, Switzerland v.8.0.1).

Biodistribution studies were performed in a Wizard 1470 Gamma Counter (Perkin Elmer). The pregnant females were sacrificed in a CO_2 chamber. Embryos were extracted and counted for 1 min in the gamma counter. Decay correction was performed and data represented as relative %ID/ g.

QUANTIFICATION AND STATISTICAL ANALYSIS

Heteroplasmy Statistical Analysis

The magnitude of heteroplasmy shifts under constant selective pressure depends on heteroplasmy levels, so percentage-point shifts observed in mice with different initial heteroplasmies cannot be directly compared. For example, for the same selective pressure, smaller percentage-point shifts are expected as the limits of 0% and 100% are approached. To allow comparison of heteroplasmy shifts across diverse samples, we use a transformation that accounts for the heterogeneity in expected shift magnitude from a given selective pressure. This transformation (Burgstaller et al., 2014; Johnston and Jones, 2016) is $\Delta h = \ln((h\ (h_0 - 1)) / (h_0\ (h - 1)))$, comparing a heteroplasmy observation h to a reference value h_0. Depending on scientific context, h_0 may be a sample taken earlier in time, or from a reference tissue: we specify the source of the corresponding reference value in the main text. Δh, the *transformed heteroplasmy shift*, then reports a normalised magnitude of heteroplasmy shift that is comparable across samples with differing h_0 values. $\Delta h = 0$ corresponds to a null hypothesis of no selective difference between mtDNA types. Cross-sample distributions of Δh values for nonzero and zero selection are typically well approximated by Gaussian distributions (Burgstaller et al., 2018).

General Statistical Analysis

Unless specified, statistical analyses and graphics were produced with GraphPad Prism 6 software. Data sets were compared by ANOVA or non-parametric analysis when corresponded. Differences were considered statistically significant at P values below 0.05. $^{*}p < 0.05$; $^{**}p < 0.01$; $^{***}p < 0.001$; $^{****}p < 0.0001$. All statistical analyses are presented as n, mean ± s.d. or mean ± s.e.m. in the figure legends.

DATA AND CODE AVAILABILITY

Some of the datasets supporting the current study have not been deposited in a public repository yet, but will be done when possible, meanwhile they are available from the corresponding author upon request.